Generation of ultrahigh magnetic fields and micro-scale particle accelerator

M. Murakami and D. Balusu
Institute of Laser Engineering, Osaka University

1. Introduction:

Laser plasma-based ion acceleration has drawn significant interest[1,2], due to their unique properties such as high directionality and laminar flow[3], spatial confinement on the order of micrometre (≈ μm) and temporal compactness (≈ ps), containing up to 10^{13} particles in a pulse duration, making them ideal for a wide range of applications including diagnostic tool in proton radiography experiments[4,5], compact particle accelerators[6,7], creation of high-energy density (HED) matter[8] and proton fast ignition[9]. In medical applications, proton beams can be used for radiation therapy[10,11] , as they deliver high dose of radiation to a particular depth (known as Bragg peak), resulting in less damage to healthy tissues unlike X-rays[12]. To attain high-quality and high-energy ion beams, various acceleration mechanism have been developed over the past few decades. These includes mechanisms such as target normal sheath acceleration (TNSA)[13,14], radiation pressure acceleration (RPA)[15–17], collisionless shock acceleration (CSA)[18,19], and coulomb exposition[20–22]. Among these mechanisms, TNSA stands out for its ease of implementation, leading to extensive studies through both simulations and experiments[23,24].

However, much work has to be done in order to achieve protons with higher kinetic energy. To enhance the transfer of laser energy to ions, it is crucial to maximize the absorption of the laser pulse by electrons. An effective approach involves engineer foil targets with structured design in the primary laser interaction region, departing from the use of flat foils. The success of the structured targets in enhancing the conversion efficiency and temperature for the laser-driven electron is noteworthy, evident in both particle-in-cell (PIC) simulation and experimental results.

Here, we present a novel ion acceleration scheme known as Expanding Nozzle Acceleration (ENA), which is achieved through target structuring. ENA employs a micro-nozzle housing a hydrogen sphere. The micro-nozzle plays a crucial role in facilitating a two-stage ion acceleration process, generating an accelerating electric field (Ex) at different locations and focusing the incident laser pulse. Illuminating the system with a laser intensity of 3 x 10^{21} W/cm^2 , remarkable results were observed, including a 6.25-fold enhancement in laser intensity onto the hydrogen sphere and protons attaining an energy of 400 Mev. This signifies a three-fold increase in proton energy compared to a planer target and a two-fold increase compared to spherical target. Notably, the maximum proton energy scales with $E_{max} \alpha\ I_0^{0.88}$, where I_0 is the laser intensity.

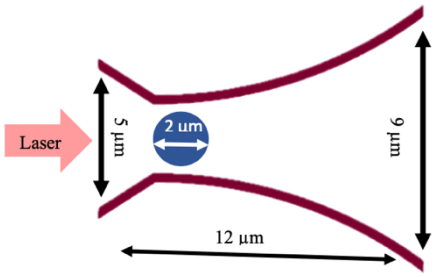

Fig. 1 : Laser and target configuration

2. Target and simulations parameters

2D PIC simulations have been performed using EPOCH. The simulation parameters are set as follows: the simulation box size is 26 μm x 26 μm, containing 2600 x 2600 cells. Each cell is filled with 100 pseudo particles for ions and 200 pseudo particles for electrons. A simulation time step of 10 fs was used.

ENA target is illustrated in the Fig.1. It comprises a hydrogen sphere with a 2 µm diameter, positioned inside the aluminum micro-nozzle, at a distance of 3 µm form the nozzle's entrance.

The nozzle has a thickness of 0.4 µm and a length of 12 µm, with an opening of 5 µm at the entrance and 9 µm at the exit. We assumed fully ionized states for the target materials, with Z = 13 for aluminum and Z = 1 for hydrogen. The number density of aluminum and hydrogen was assumed to be $35n_c$ and $30n_c$, respectively, while for electron it is $472n_c$, where $n_c = (m_e\omega_0^2/4\pi e^2)$ is the critical density. The target is irradiated with a p-polarized laser pulse with Gaussian profile both spatially and temporally, moving along the positive x-direction. The laser had a wavelength of 800 nm and a pulse duration of 100 fs (FWHM), focused to a spot size of 10 µm with a peak intensity of 3 x 10^{21} w/cm^{-2}.

When the laser incident on the target, the center part of the laser get focused by the entrance cone like structure and hot electron are generated from the inner surface. With the laser intensity 3 x 10^{21} w/cm^2 , the amplitude of the electric field 1.5 x 10^{14} V/m has amplified to 4 x 10^{14} V/m, 2.5 x amplification in electric filed and corresponding 6.25 x enhancement in laser intensity. This intensity is focused on the hydrogen sphere. The first part of the ENA target helps in increasing the intensity of the incident laser and generation of hot electrons from the inner surface, which passes through the hydrogen sphere leading to charge separation and enhances the sheath electric file (Ex) developed on the surface of the sphere.

3. Optimization of the micro-nozzle

The outer part of the laser falls on the exit arms of the target and hot elections are realized into the vacuum results is generation of electric field (Ex) at the exit arms due to the charge separation as the electron from the target moves into the vacuum, figure 3a to 3d shows the electric field (Ex) profile on the hydrogen sphere and at the exit arms of the target at different time steps. Initially, protons are accelerated by the sheath electric filed generated on the hydrogen sphere. These accelerated protons then enter into the electric field generated at the exit arms of the target and undergo further accelerates. Proton density profile of at different time steps is shown in the Fig. 2.

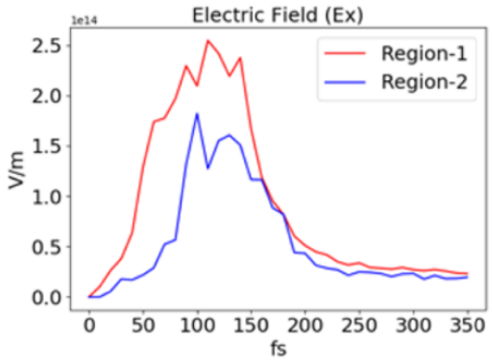

Fig. 2: Temporal evolution of the electric field.

For the effective proton acceleration, the position of the hydrogen sphere inside the micro-nozzle plays an important role. The protons that are accelerated from the electric field in the region-1, must be properly timed to undergo further acceleration from the electric filed generated in the region-2.

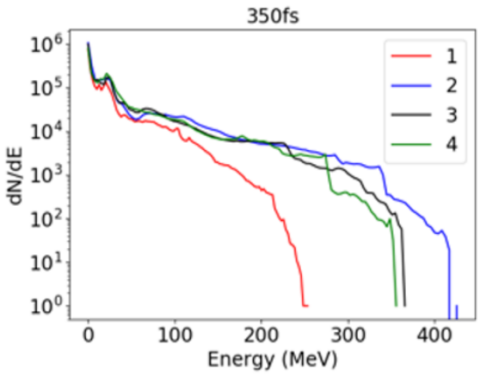

Fig. 3: Energy spectrum for the different positions.

Figure 3 shows the energy spectrum on the protons for different positions of the hydrogen sphere inside the micro-nozzle. Initially center of the hydrogen sphere is kept inside the nozzle at distance of 3 µm from the entrance and shifted 1 µm towards the nozzle exit, it was observed that kinetic energy of the protons

is high when center of the hydrogen sphere at a distance of 4 μm from the nozzle entrance

We have compared the ENA target with planar target and a hydrogen sphere without the micro-nozzle. It was observed that three-fold increase in the energy of the proton compared to planer target, and a two-fold increase in proton energy compared to hydrogen sphere without the outer micro-nozzle.

Figure 6a show the energy spectrum of proton for all the three cases at 400 fs and Fig.6b shows the evolution of proton energy over time. For the ENA target, the proton energy drastically increased from 100 fs to 250 fs, attributed to its two-stage acceleration that sets up electric field (Ex) at different locations. This provides an additional accelerating field for the initially accelerated proton from the hydrogen sphere. In contrast, for planer and spherical target, protons experience initial acceleration due to electric filed established by charge separation, but they lack a further driving force. As a result, kinetic energy of the protons saturates quickly. This marked difference highlights the crucial role of the micro-nozzle in driving ion acceleration.

To explore the intensity dependency across a broader spectrum, additional simulations were performed with seven different intensities. The outcome of these simulations was utilized to establish a preliminary intensity-scaling, as illustrated in the fig. Analysis of the data points reveals that the maximum proton energy scales with $E_{max}\alpha\ I_0^{0.88}$ for intensities greater then 5 x 10^{20} W/cm^2 and less then 5 x 10^{21} W/cm^2, and $E_{max}\alpha\ I_0^{0.5}$ for intensities less then 5 x 10^{20} W/cm^2. However, for intensities greater then 5 x 10^{21} W/cm^2, target distortion occurs due to the extremely high intensities, potentially leading to decreased performance. Consequently, parameters of the target are scaled up for such high intensities. Hence for the given parameters the ideal intensities for irradiating the ENA target is between 5 x 10^{20} W/cm^2 to 5 x 10^{21} W/cm^2.

Comparing our finding to the intensity scaling of Target Normal Sheath Acceleration (TNSA) with $E_{max}\alpha\ I_0^{0.5}$, Expanding nozzle acceleration (ENA) performance demonstrates improvement with $E_{max}\alpha\ I_0^{0.88}$ for higher intensities. However, at lower intensities, ENA performance aligns with TNSA.

4. Conclusion:

In this study, we have introduced a novel ion acceleration scheme, Expanding Nozzle Acceleration (ENA). With this scheme, protons undergo acceleration from the electric field generated at two different locations. The utilization of ENA reveals significantly higher proton energies compared to the conventional schemes, as demonstrated by 2-dimensional PIC code EPOC. Specifically, ENA exhibits a two-fold enhancement in proton energy compared to spherical target and three-fold enhancement in proton energy compared to planer target. Moreover, the maximum proton energy in ENA scales with $E_{max}\alpha\ I_0^{0.88}$. This scheme still leaves further optimization for higher proton energy, but at the price the energy efficiency. A proof-of-principle experiment for ENA is expected to be demonstrated under a moderate laser condition.

Reference

1. A. Macchi, M. Borghesi, and M. Passoni, Rev. Mod. Phys. **85**(2), 751–793 (2013).

2. B.M. Hegelich, B.J. Albright, J. Cobble, K. Flippo, S. Letzring, and H. Ruhl, Nature **439**(7075), 441–444 (2006).

3. T.E. Cowan, J. Fuchs, H. Ruhl, A. Kemp, E. Brambrink, A. Newkirk, H. Pépin, and N. Renard-LeGalloudec, Phys. Rev. Lett. **92**(20), 204801 (2004).

4. L. Romagnani, J. Fuchs, M. Borghesi, P. Antici, P. Audebert, F. Ceccherini, T. Cowan, T. Grismayer, S.

Kar, A. Macchi, A. Schiavi, T. Toncian, and O. Willi, Phys. Rev. Lett. **95**(19), 195001 (2005).

5. M. Borghesi, A. Schiavi, D.H. Campbell, M. Galimberti, L. Gizzi, R.J. Clarke, and S. Hawkes, Applied Physics Letters **82**(10), 1529–1531 (2003).

6. K. Krushelnick, E.L. Clark, M. Zepf, J.R. Davies, F.N. Beg, A. Machacek, M.I.K. Santala, M. Tatarakis, I. Watts, P.A. Norreys, and A.E. Dangor, Physics of Plasmas **7**(5), 2055–2061 (2000).

7. A. Pukhov, "Three-Dimensional Simulations of Ion Acceleration from a Foil Irradiated by a Short-Pulse Laser," Phys. Rev. Lett. **86**(16), 3562–3565 (2001).

8. P. Patel, A. Mackinnon, M. Key, T. Cowan, M. Foord, M. Allen, D. Price, H. Ruhl, P. Springer, and R. Stephens, Phys. Rev. Lett. **91**(12), 125004 (2003).

9. M. Roth, T.E. Cowan, J. Johnson, F. Pegoraro, S.V. Bulanov, E.M. Campbell, M.D. Perry, and H. Powell, Phys. Rev. Lett. **86**(3), 436–439 (2001).

10. S.V. Bulanov, H. Daido, T.Z. Esirkepov, V.S. Khoroshkov, J. Koga, K. Nishihara, F. Pegoraro, T. Tajima, and M. Yamagiwa, (n.d.).

11. E. Fourkal, J.S. Li, M. Ding, T. Tajima, and C. -M. Ma, Medical Physics **30**(7), 1660–1670 (2003).

12. W.D. Newhauser, and R. Zhang, Phys. Med. Biol. **60**(8), R155–R209 (2015).

13. R.A. Snavely, M.H. Key, S.P. Hatchett, T.E. Cowan, M. Roth, T.W. Phillips, A. MacKinnon, Phys. Rev. Lett. **85**(14), 2945–2948 (2000).

14. S.C. Wilks, A.B. Langdon, T.E. Cowan, M. Roth, M. Singh, S. Hatchett, M.H. Key, D. Pennington, A. MacKinnon, and R.A. Snavely, Physics of Plasmas **8**(2), 542–549 (2001).

15. B. Qiao, M. Zepf, M. Borghesi, and M. Geissler, Phys. Rev. Lett. **102**(14), 145002 (2009).

16. A. Henig, S. Steinke, M. Schnürer, T. Sokollik, R. Hörlein, D. Kiefer, J. Meyer-ter-Vehn, T. Tajima, P.V. Nickles, W. Sandner, and D. Habs, Phys. Rev. Lett. **103**(24), 245003 (2009).

17. B. Gonzalez-Izquierdo, R. Capdessus, M. King, R. Gray, R. Wilson, R. Dance, J. McCreadie, N. Butler, S. Hawkes, J. Green, N. Booth, M. Borghesi, D. Neely, and P. McKenna, Applied Sciences **8**(3), 336 (2018).

18. L.O. Silva, M. Marti, J.R. Davies, R.A. Fonseca, C. Ren, F.S. Tsung, and W.B. Mori, Phys. Rev. Lett. **92**(1), 015002 (2004).

19. F. Fiuza, A. Stockem, E. Boella, R.A. Fonseca, L.O. Silva, D. Haberberger, S. Tochitsky, C. Gong, and C. Joshi, Phys. Rev. Lett. **109**(21), 215001 (2012).

20. K. Nishihara, H. Amitani, M. Murakami, S.V. Bulanov, and T.Zh. Esirkepov, Nucl. Instruments and Methods in Physics Research Section A **464**(1–3), 98–102 (2001).

21. M. Murakami, and K. Mima, Phys. Plasmas **16**(10), 103108 (2009).

22. T. Nakamura, S.V. Bulanov, H. Daido, T. Esirkepov, T. Pikuz, A.S. Pirozhkov, M. Tampo, and A. Yogo, Phys. Plasmas **16** (10), 103108 (2009)..

23. F. Wagner, O. Deppert, C. Brabetz, A. Tebartz, B. Zielbauer, M. Roth, T. Stöhlker, and V. Bagnoud, Phys. Rev. Lett. **116**(20), 205002 (2016).

24. F. Wagner, S. Bedacht, V. Bagnoud, O. Deppert, S. Geschwind, R. Jaeger, A. Ortner, A. Tebartz, B. Zielbauer, D.H.H. Hoffmann, and M. Roth, Phys. Plasmas **22**(6), 063110 (2015).